Enthalpy Recovery of Poly(ether imide): Experiment and Model Calculations Incorporating Thermal Gradients

Sindee L. Simon

Department of Chemical Engineering, University of Pittsburgh, Pittsburgh, Pennsylvania 15261

Received September 30, 1996; Revised Manuscript Received April 14, 1997[⊗]

ABSTRACT: Enthalpy recovery data on poly(ether imide) from differential scanning calorimetry (DSC) is fit using the Moynihan−Tool−Narayanswamy model of structural recovery. A self-consistent phenomenological equation is used to describe the experimentally observed structure and temperature dependence of the relaxation time in both glass and equilibrium regimes. Temperature gradients in the DSC sample are calculated based on the thermal diffusivity of the material and are, for the first time, incorporated into the model calculations. When no thermal gradients are assumed, model parameters are found to vary with thermal history despite the use of the self-consistent equation for the relaxation time. There is also a discrepancy between experimental data and model calculations with respect to the shape of the DSC annealing peaks. Accounting for the presence of thermal gradients in the DSC sample is found to affect the values of the model parameters needed to fit the data. However, thermal gradients are unable to account for the thermal history dependence of the model parameters or for the discrepancy between observed and calculated shapes of DSC annealing peaks.

Introduction

Mathematical models of structural recovery[1−7] have been successful in predicting the behavior of glass-forming materials and for providing a physical understanding of that behavior. The models are capable of describing manifestations of the glassy response such as the rate dependence of T_g, structural recovery, the asymmetry of approach to equilibrium,[2] and the results of differential scanning calorimetry (DSC) enthalpy recovery experiments.[8−10] However, there are unresolved issues pertaining to the models,[4,7,11] including an apparent dependence of model parameters on thermal history. A recent discussion meeting at an international conference on glasses[12] was devoted to identifying these problems. Possible reasons for the problems may be (1) the presence of thermal gradients,[13,14] (2) an inconsistent equation for describing the effects of temperature and structure on the relaxation time, or (3) incorrect representation of structural recovery using the Kohlrausch−William−Watts (KWW)[15,16] function.[4] In this work, we show that the first two issues identified are not responsible for the discrepancies noted. This is important because it implies that future modifications of the model must deal with other issues, such as the adequacy of the KWW representation.

The presence of thermal gradients in differential scanning calorimetric measurements was suggested to be a factor in discrepancies between experimental data and model calculations by Hodge and Huvard in the early 1980s.[14] The researchers used Moynihan's formulation[3] of the Tool−Narayanaswamy model and found good agreement between calculated and observed values for the magnitude and placement of annealing peaks at low degrees of annealing (small overshoot peaks at T_g) using a single set of model parameters. However, for high degrees of annealing (large overshoots), calculations using the same model parameters overpredicted the magnitude of annealing peaks. The researchers postulated that these differences might be attributable to thermal lag effects.

Several years later, Hutchinson and co-workers[15] also ascribed deviations in DSC measurements to thermal lag effects. In their work, they found that as cooling and heating rates were increased, at a constant ratio of the two rates, DSC annealing peaks broadened and flattened, whereas the KAHR model[2] and the Tool−Narayanaswamy model[17] predict that the shape of the curves should be the same when the ratio of cooling to heating rates is held constant. Hutchinson et al. then developed a correction for DSC data based on the assumption that the model is correct and that the deviations observed between experimental data and calculations are due to thermal lag.

More recently, O'Reilly and Hodge[18] found that model parameters varied with thermal history even for relatively slow heating rates (1.25 °C/min) where thermal gradients were assumed to be negligible. Their results indicate that thermal gradients cannot account for all of the shortcomings of the model. In this work, we go one step further and determine the effect of thermal gradients on the shape of calculated enthalpy recovery curves for typical heating rates (10 °C/min) by incorporating thermal gradients into the model.

There are two thermal effects which could impact the agreement between calculated and experimental heat capacity curves. The first is the thermal resistance between the sample and DSC instrument.[4,14,19−21] This effect is not addressed in this work since thermal resistance can be minimized by using a silicon grease with a high thermal conductivity between the sample pan and furnace, by insuring that the sample pan is flat and that the sample is in good contact with the pan, and by using proper calibration procedures.[4] The effects of thermal gradients in the sample, on the other hand, are of interest. Such gradients have been estimated by various researchers by placing melting standards above and below the sample in the DSC pan and measuring the differences in the observed melting temperatures.[4,14,22,23] The difference between the melting temperature of the standard on the bottom and top of the sample pan is generally reported to be on the order of 1 °C and to increase with increased rate of heating.[4,14,22,23] Another technique[19] for estimating thermal lag involves equilibration of the sample at an initial temperature followed by a temperature ramp to a second temperature. The time lag for the heat flow to return to steady

[⊗] Abstract published in *Advance ACS Abstracts,* June 1, 1997.

S0024-9297(96)01450-7 CCC: $14.00

state at the second temperature is indicative of the thermal lag in the sample and was reported[19] to increase with sample size, heating rate, and temperature. Using this method, the thermal lag at 16 °C/min was found[19] to range from 2.7 to 3.6 °C for a 66 mg sapphire disk at temperatures from 350 to 750 K.

In the present work, we first review the Tool−Narayanswamy model of structural recovery; then we present analytical and numerical solutions for the temperature profile in the DSC sample. We then incorporate the calculated temperature gradient into the model of structural recovery and fit new experimental DSC data for poly(ether imide) with the modified model. We will compare the fit of the modified and unmodified models and show that incorporating thermal gradients does not significantly impact the fit of the model to experimental data although it does impact the values of the fitting parameters obtained.

Tool−Narayanaswamy Model of Structural Recovery

Models of structural recovery are based on work done originally by Narayanaswamy[1] and account for both the nonlinearity and the nonexponentiality of the process. Moynihan's formulation[3] of the Tool−Narayanaswamy model is used here; a brief description follows. In Moynihan's equations, the fictive temperature, T_f, originally defined by Tool,[24] is used as a measure of the structure of the glass. The evolution of fictive temperature is both nonlinear and nonexponential and is represented by the generalized KWW[15,16] function

$$\frac{dT_f}{dT} = 1 - \exp\int_0^t -(dt/\tau_o)^\beta \qquad (1)$$

The nonexponentiality of the process is described by β; the nonlinearity is incorporated into the model by allowing the relaxation time τ_o to be a function of both temperature and structure (T_f). Equation 1 is solved numerically for a given thermal history which begins at a temperature T_o above T_g

$$T_{f,n} = T_o + \sum_{i=1}^{n} \Delta T_i \left\{1 - \exp\left[-\left(\sum_{j=1}^{n} \frac{\Delta T_j}{q\tau_{o,j}}\right)^\beta\right]\right\} \qquad (2)$$

where $T_{f,n}$ is the fictive temperature after the nth temperature step, ΔT_i is the temperature step, and q is the rate of the DSC temperature ramp experiment which is being modeled. In this work, the temperature steps are taken to be 1 K in the equilibrium regime and deep in the glass, and 0.25 K in the glass transition region where enthalpy recovery is observed.

Equation 2 describes the evolution of the fictive temperature as a function of time in a specified thermal history consisting of cooling and heating ramps. To compare the calculation to experimental DSC data, the heat capacity is calculated from the temperature derivative of the fictive temperature[25]

$$C_p(T) = C_{pg}(T) + \Delta C_p(T_f)\frac{dT_f}{dT} \qquad (3)$$

where $C_{pg}(T)$ is the glass heat capacity and $\Delta C_p(T_f)$ is the difference between the liquid and glass heat capacities extrapolated to temperatures T and T_f, respectively. The assumption that $\Delta C_p(T) = \Delta C_p(T_f)$ is often used in calculating the normalized heat capacity since the error entailed is generally less than 10%. However, for large annealing peaks, a change in the maximum height of the annealing peak by 10% can significantly affect the value of the parameters needed to fit the curve;[4] hence, eq 3 is used in this work.

A phenomenological equation relating the relaxation time τ_o to temperature and structure (T_f) is needed to perform the model calculations. The Tool−Narayanaswamy equation[1] is an Arrhenius-like equation, and although it is widely used, it is unable to describe the observed Vogel−Tammann−Fulcher[26] (WLF[27]) behavior in the equilibrium limit when $T_f = T$. Hence, an equation derived by Sherer,[28] based on Adam and Gibbs' approach,[29] is used in this work

$$\ln \tau_o = \ln A + \frac{D/RT}{\left[a \ln\left(\frac{T_f}{T_2}\right) + b(T_f - T_2)\right]} \qquad (4)$$

or

$$\ln a_T = \ln \frac{\tau_o}{\tau_{o,ref}} = \frac{D/RT}{\left[a \ln\left(\frac{T_f}{T_2}\right) + b(T_f - T_2)\right]} - \frac{D/RT_{ref}}{\left[a \ln\left(\frac{T_{ref}}{T_2}\right) + b(T_{ref} - T_2)\right]} \qquad (5)$$

where D/Ra, b/a, T_2, and $\ln \tau_{o,ref}$ are treated as fitting parameters, and $\ln a_T$ is the temperature shift factor. Sherer's equation is derived assuming that ΔC_p is related to the configurational entropy and that it is a linear function of temperature. According to the derivation, the constants a and b in the above equation would be given by $\Delta C_p(T) = a + bT$. However, DiMarzio and Dowell[30] have shown that the configurational portion of the heat capacity change at T_g is on the order of 75% of the total change; Goldstein[31] and Roe[32] have also shown that the configurational portion of the heat capacity change at T_g can be much smaller than the total value. Hence, it is not expected that the temperature dependence of the configurational portion of the change in heat capacity will necessarily be the same as the temperature dependence of the total change in heat capacity. Further, the value of ΔC_p has an error of approximately ten times the errors in the glass and liquid heat capacities, C_{pg} and C_{pl}, respectively, since the absolute errors in C_{pg} and C_{pl} are additive and the value of ΔC_p is approximately ten times smaller than that of C_{pg} and C_{pl} for PEI (see later). For these reasons, the value of b/a is taken as a fitting parameter rather than as an experimentally determined value.

The parameters D/Ra, b/a, and T_2 are determined from data previously published[33] in which enthalpy, volume, and creep recovery measurements for poly(ether imide) were reported at various temperatures. Time−temperature superposition of the normalized data resulted in reduced curves and gave the temperature dependence of the shift factor ($\log a_T$) in the equilibrium regime where $T = T_f$. A time-temperature reduction of the nonnormalized enthalpy data also gave a reduced curve and the temperature dependence of the shift factor at constant T_f. The fit of eq 5 to the described shift factor data is shown in Figure 1, where D/Ra =780, b/a = −1/580 K and T_2 = 152.6 °C. The reference temperature is 207.5°C. Other phenomenological equations reported in the literature were tested for their

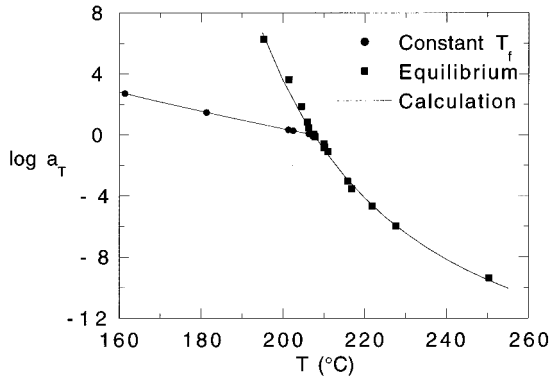

Figure 1. Temperature dependence of the shift factors obtained in previous work.[33] The equilibrium shift factors were obtained by time−temperature superposition of normalized enthalpy, volume, and creep recovery measurements taken at various temperatures. The isostructural (constant T_f) shift factors were obtained by time-temperature superposition of fictive temperature vs log time curves at various temperatures. Both curves are fit by Sherer's equation using one set of parameters.

ability to fit the shift factor data in Figure 1; the equations by Tool−Narayanswamy,[1] Hodge,[34] Matsuoka,[35] and Spathis[36] were found to be incapable of describing the data with only one set of parameters.

The presence of a thermal gradient in the sample was incorporated into the Moynihan−Tool−Narayanaswamy model of structural relaxation by calculating the fictive temperature at several points in the sample and averaging the response. Although it is possible to calculate the temperature profile in the sample within the structural recovery calculation, the two operations were accomplished independently in this work for simplicity. First, the temperature profile and average temperature in the DSC sample were calculated as a function of program temperature for a given thermal history, as described below. Then the structural recovery was calculated at various points in the sample and averaged to give the sample response at the program temperature T_p, $(dT_f/dT)_{T_p}$

$$\left(\frac{dT_f}{dT}\right)_{T_p} = \int_0^1 \left(\frac{dT_f}{dT}\right) d\xi \tag{6}$$

where ξ is the normalized distance from the bottom to the top of the sample.

Analytical Results−Calculation of Temperature Profile

The temperature profile in the DSC sample is determined analytically for the ideal case in which the top and bottom of the sample pan are assumed to be maintained at the program temperature (T_p). The one-dimensional heat conduction equation,[37] in which radial heat transfer is neglected, is used to estimate the temperature profile in the sample

$$\frac{\partial}{\partial x}\kappa\frac{\partial T}{\partial x} = \rho C_p \frac{\partial T}{\partial t} \tag{7}$$

where κ is the thermal conductivity, ρ is the density, and C_p is the heat capacity of the material. If the thermal diffusivity ($k = \kappa/\rho C_p$) is assumed to be a constant, the heat conduction equation can be solved analytically for the temperature profile during a single temperature ramp for the ideal case

$$T(x,t)_{\text{ideal}} = T_p(t) - \frac{4L^2 m}{k}\sum_{n=1}^{\text{odd}} \frac{(1 - e^{-(n\pi)^2 tk/L^2})}{(n\pi)^3}\sin\left(\frac{n\pi x}{L}\right) \tag{8}$$

where L is the height of the sample, m is the ramp rate, k is the thermal diffusivity, t is the time from the start of the ramp, and x is the distance from the bottom of the sample. See Appendix for derivation.

The thermal conductivity and heat capacity were assumed to be independent of temperature for the analytical solutions. This is not observed experimentally; instead, the thermal conductivity shows a downward step change as the temperature is increased through T_g, and the heat capacity shows an upward step change. The step change in thermal diffusivity for PEI at T_g cannot be calculated because the step change in thermal conductivity at T_g has not been measured and is not reported in the literature. Sufficient data is, however, available for polystyrene; on the basis of literature values of polystyrene's density,[38] heat capacity,[39] and thermal conductivity,[40] the decrease in thermal diffusivity at T_g is 50%.

The heat conduction equation is also solved numerically for the ideal and nonideal cases in which the thermal diffusivity of PEI is assumed to decrease by 50% through T_g. The numerical calculation is carried out by taking small time and position steps:

$$T(x_i,t_j) = T(x_i,t_{j-1}) + \frac{k(T)\Delta t[T(x_{i-1},t_{j-1}) + T(x_{i+1},t_{j-1}) - 2T(x_i,t_{j-1})]}{(\Delta x)^2} \tag{9}$$

To obtain the above equation from the heat conduction equation, it was assumed that the thermal conductivity is not a function of position in the sample, i.e., $(\partial/\partial x)\kappa(\partial T/\partial x) = \kappa(\partial^2 T/\partial x^2)$. This assumption is obviously valid in the glassy and equilibrium states where the thermal conductivity is not a strong function of temperature; it was found to also be a good approximation in the transition range, resulting in an error of less than 10% in this regime. The numerical calculations are stable when $k\Delta t/(\Delta x)^2 \leq 0.5$. In the work presented, the sample was divided into 10 steps, so Δx was taken to be 10%L (=0.1 mm) for the 1.0 mm sample modeled. A time step, Δt, of 0.147 s = $0.5(\Delta x)^2/k$ was used to insure agreement between numerical and analytic solutions for the case where k is constant and equal to the glassy value (=0.00034 cm^2/s based on the literature value of the thermal conductivity[41] and the values of the density and heat capacity obtained experimentally).

Figure 2 shows the ideal temperature profiles in a DSC sample during heating at 10 °C/min from far below T_g to above T_g at various temperatures. Two calculations are shown: the analytical one in which the thermal diffusivity was assumed to be independent of temperature and equal to the glassy value and the numerical calculation in which the thermal diffusivity was assumed to decrease by 50% through the glass temperature. In Figure 2, the calculated temperature difference between the program and sample temperature is shown as a function of distance from the sample pan bottom for various program temperatures. As expected, the temperature profiles are symmetric due to the assumption that the top and bottom of the sample were both maintained at the program temperature. When the thermal diffusivity is independent of temper-

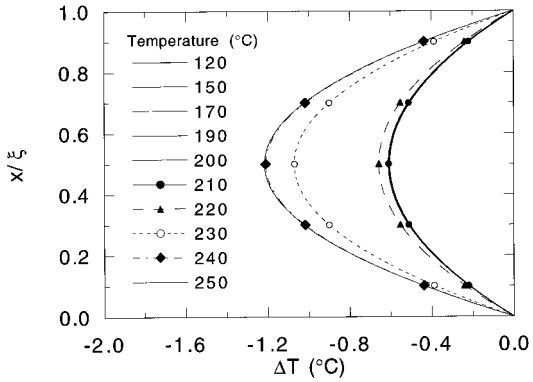

Figure 2. The temperature profile during heating at 10 °C/min after cooling at 0.1 °C/min for the ideal case where the top and bottom of the sample are assumed to be at the program temperature. The *y*-axis is normalized distance from the bottom of the sample ($\xi = 0$ is the sample bottom, $\xi = 1$ is the sample top). The *x*-axis gives the difference between the program temperature and the sample temperature. The temperature profile is independent of temperature in the glassy state ($T \leq 210$ °C). The thermal lag increases as the temperature rises through T_g. The profile is independent of temperature in the equilibrium region ($T \geq 240$ °C).

ature, the temperature profile is the same at all temperatures, showing a maximum temperature lag in the center of the sample of 0.6 °C, with the average sample temperature being 0.4 °C lower than the program temperature. The analytical and numerical calculations agree in this regime. On the other hand, when the thermal diffusivity was assumed to decrease by 50% through T_g, there is a corresponding increase in the thermal lag at the center of the sample above T_g to a value of 1.2 °C, with the average sample temperature being 0.8 °C lower than the program temperature. It is reiterated that these results are for the ideal case and are conservative estimations of the thermal gradients in the sample.

Now that we have calculated the temperature profiles in the sample for the ideal temperature gradient, we can use the structural recovery model coupled with eq 6, to calculate the response of the sample to a temperature ramp. This methodology assumes that the ramp rate that the sample sees is constant (i.e., the rate of temperature change within the sample is not a function of position). This assumption is valid: the temperature profile calculations, shown in Figure 2, indicate that the temperature profile in the sample is independent of temperature in the glass and equilibrium regimes and changes over a 15 °C range in the transition region. All parts of the sample, then, experience the same ramp rate in the glass and equilibrium regions, and the ramp rate through the transition region deviates by only 5% from that of the program temperature for cooling or heating rates of 10 °C/min. It is noted that there is an initial lag at the beginning of a heating or cooling ramp before the steady state temperature profile is reached. During this initial period, the heating or cooling rates will differ throughout the sample. The magnitude of the lag increases with heating or cooling rate, and was calculated to be less than 10 °C for rates of or below ±30 °C/min for PEI. The initial lag was not incorporated into the calculations because the upper and lower temperature limits are high and low enough, (being 50 °C above and 110 °C below T_g, respectively) that the steady state profile is reached before vitrification occurs on cooling and before enthalpy recovery begins on heating. In the event that different parts of the sample see different heating and/or cooling rates, the calculations need to take this into account through the parameter *q* in eq 2, which would need to be the heating or cooling rate experienced by the sample at position *x*.

Experimental Procedure

Poly(ether imide) (PEI), an amorphous engineering thermoplastic, Ultem 1000 from General Electric, was used. Its chemical structure is shown below.

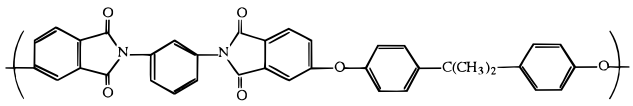

The material has a glass temperature of approximately 206 °C at a cooling rate of 0.25 °C/min based on dilatometric measurements.[42] The number average molecular weight of the material is 45 000 with a polydispersity index of 2.0, based on a room temperature gel permeation chromatography measurement in 1-methyl-2-pyrrolidinone using polystyrene standards for calibration.

A Perkin-Elmer DSC 7, equipped with a custom-designed water cooling system which yields a stable and reproducible baseline, was used to determine the heat capacity of the poly(ether imide) in the glass and equilibrium regimes during cooling at rates of 10, 20, and 30 °C/min. The runs were made under nitrogen purge. One sample weighing 10 mg was used. The weights of sample and reference pans were matched to within 0.01 mg. The temperature and heat flow of the instrument was calibrated on cooling using a liquid crystal, *N*-(4-(*n*-octyloxy)-2-hydroxybenzal)-4′-*n*-butylaniline,[43] which does not undercool. Calibration of the absolute heat capacity was performed, also on cooling, using corundum (synthetic sapphire).

The same Perkin-Elmer DSC 7, equipped with a custom-designed water cooling system, was used to measure enthalpy recovery during heating at 10 °C/min after cooling from 240 to 100 °C at six rates ranging from 0.1 to 30 °C/min. For these measurements, indium was used to calibrate the temperature and heat flow on heating at 10 °C/min. The baseline stability was such that the six scans could be superposed in both glass and liquid regions with simply a vertical shift.

The sample is thermally stable in the temperature range studied, and the physical aging phenomena is physically reversible by heating to 240 °C. These points are confirmed by the fact that the fictive temperature obtained on heating after a given cooling rate from 240 °C is unchanged before and after the experiments are performed.

Results

Measurement of Heat Capacity. The heat capacity in the glass and liquid states is needed to transform the calculated normalized heat capacity to the nonnormalized value (through eq 3) in order to compare calculations to experiment. The values of C_{pg} and C_{pl} were found to not depend on cooling rate for the cooling rates studied and to be reproducible for the three runs to within 2%:

$$C_{pg}(T) = 0.94 + 0.0034T\ (°C) \quad \text{from 125 to 165 °C} \quad (\text{J/(g °C)}) \quad (12)$$

$$C_{pl}(T) = 1.51 + 0.0017T(°C) \quad \text{from 230 to 285 °C} \quad (\text{J/(g °C)}) \quad (13)$$

The change in $\Delta C_p(T)$ at T, needed to convert the calculated normalized heat capacity to the heat capacity (see equation 3) is determined by difference of equations (13) and (12), respectively:

$$\Delta C_p(T) = C_{pl}(T) - C_{pg}(T) = 0.57 - 0.0017T(°C) \quad (\text{J/(g °C)}) \quad (14)$$

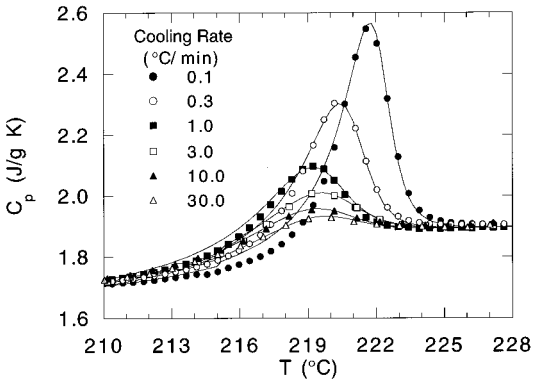

Figure 3. Experimental (data points) and calculated (lines) enthalpy recovery for heating at 10 °C/min after cooling at various cooling rates ranging from 0.1 °C/min to 30 °C/min. Temperature gradients were not incorporated into the calculations. Model parameters for the calculated curves were determined such that the height and placement of the annealing peaks corresponded to the experimentally observed values. In a previous manuscript,[33] similar DSC scans were shown but as a function of aging time; in that work although the *y*-axis read C_p, the value reported was not an absolute heat capacity—i.e., the *y*-axis was shifted relative to the absolute value. The C_p values reported here are correct.

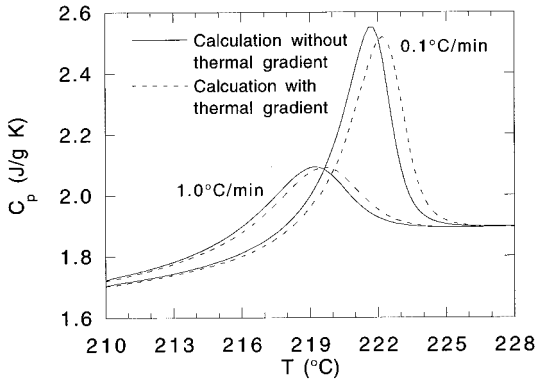

Figure 4. Calculated enthalpy recovery curves for heating at 10°C/min after cooling at 0.1 and 1.0 °C/min. The results are shown for two calculations, one incorporating no thermal gradient and the other incorporating an ideal thermal gradient. Model parameter values are the same as those used in Figure 3. Incorporating thermal gradients results in the annealing peak being shifted to higher temperatures. A slight broadening of the peak is also observed.

Since the value of ΔC_p is based on extrapolation of the glass and liquid heat capacities to T_g, eq 14 is expected to only be valid near T_g. The apparent linear temperature dependence of $\Delta C_p(T)$ is obtained simply because C_{pg} and C_{pl} have linear temperature dependences in the range measured. The real temperature dependence of ΔC_p has been suggested to be somewhere between a hyperbolic temperature dependence and no temperature dependence.[4]

Data for the heat capacity of poly(ether imide) obtained by DSC during heating has been tabulated by Hay et al.[44] for an unspecified thermal history and DSC heating rate. The value of $\Delta C_p(T_g)$ reported in the present work obtained on cooling rather than heating is within 2% of their value, and the absolute values of C_p are within 10% of their values over the temperature range they studied. If the difference in T_g is accounted for, the differences in C_p are considerably less. The temperature dependence of the rubbery heat capacity does differ between the two papers, and it is not clear why although our data cover a significantly broader temperature range.

We note that, in this present study, the same sample and the same heating rate were used for all experiments. Hence, any errors in C_p will be systematic errors. Such errors may affect the absolute value of the model parameters needed to fit the data since the heat capacities in liquid and glassy states are needed to translate the normalized heat capacity calculated in the model to the nonnormalized value. However, any systematic errors present are not expected to affect the dependence of the model parameters on thermal history, the latter of which is the focus of this work.

Structural Recovery. Experimental DSC heating curves are shown by the data points in Figure 3 for various cooling rates, ranging from 0.1 to 30 °C/min. For ease of presentation, not all of the data points obtained during each scan are shown. The annealing peaks observed in the DSC heating scans increase and move to higher temperatures as the cooling rate decreases. This has been described in detail by other authors.[3,7,45] It is emphasized that the annealing peak temperature does not correspond to T_g but depends on the thermal history as described by the models of structural recovery.

Table 1. Dependence of Model Parameters on Cooling Rate for Calculations Made without Incorporating Thermal Gradients

q (°C/min)	β	$\tau_{o,ref}$
0.1	0.322	8000
0.3	0.347	6000
1.0	0.369	7000
3.0	0.406	11000
10.0	0.455	11000
30.0	0.500	13000

The fit of the Moynihan−Tool−Narayanswamy model, without the incorporation of temperature gradients, is also shown in Figure 3. The values of the two model parameters ($\tau_{o,ref}$ and β) used to fit each curve were determined such that the height and placement of the calculated annealing peak corresponded to the experimentally observed value. The values, particularly β, depend on the thermal history despite the fact that a self-consistent equation was used to describe the effects of temperature and structure on the relaxation time, as shown in Table 1.

Figure 3 also shows another, albeit relatively minor, problem with the model calculations in that there appears to be a deviation between the shapes of the calculated and experimental peaks: the calculated curve is shifted above the experimental curve at temperatures below the peak temperature and the reverse is observed, above the peak. In other words, the calculation predicts that enthalpy recovery will begin and end at a temperature lower than that experimentally observed. It is noted that this latter discrepancy is usually present in the calculations of other researchers, although depending on the scale of the presented results, it may not be very noticeable.

The effect of incorporating a thermal gradient in the calculation is shown in Figure 4 for cooling rates of 0.1and 1.0 °C/min, respectively. Two calculated curves are shown for each cooling rate, one incorporating thermal gradients and the other not. Both calculations, with and without thermal gradients, were made using the same set of model parameters (those used in the calculations in Figure 3). The presence of a thermal gradient shifts the calculated response to higher temperatures and slightly broadens the response. The height of the annealing peak is also lowered.

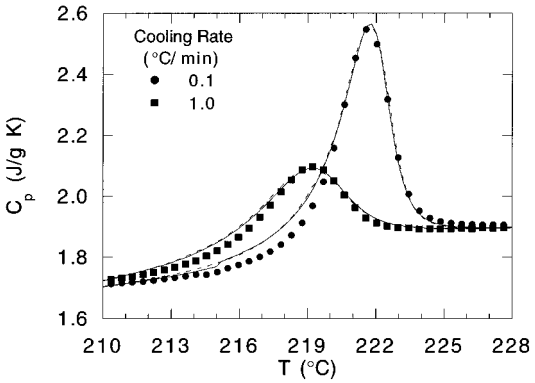

Figure 5. Experimental data (points) for heating after cooling at 0.1 and 1.0 °C/min. Two calculations are shown for each cooling rate: one incorporating no thermal gradient (solid line) and the other incorporating an ideal thermal gradient (dashed line). Model parameters were determined such that the height and placement of the annealing peaks corresponded to the experimentally observed values. No significant difference can be discerned between the fits of the calculations with and without thermal gradients.

Table 2. Dependence of Model Parameters on Cooling Rate for Calculations Made Incorporating Thermal Gradients

q (°C/min)	β	$\tau_{o,ref}$
0.1	0.325	5500
0.3	0.350	5000
1.0	0.369	4500
3.0	0.408	7500
10.0	0.460	7500
30.0	0.502	10000

To determine whether thermal gradients in the sample could account for the deviations observed between the calculated and experimental curves, the model parameters were varied in order that the height and placement of the calculation incorporating the thermal gradient fit the experimental peak. There is no significant difference between the calculation assuming no thermal gradients and that assuming an ideal gradient, as shown in Figure 5 with experimental data for cooling rates of 0.1and 1.0 °C/min (i.e., the two calculated curves are indistinguishable except for a slight broadening of the calculated curves incorporating thermal gradients). In order to match the height and placement of the observed annealing peak for the cooling rate of 0.1 °C/min, $\tau_{o,ref}$(207.5 °C) was decreased to 5500 s and β was increased slightly to 0.325,[46] changes of 30% and 1%, respectively, compared to the values used in the calculation without a thermal gradient. Similar changes in model parameters were found for other cooling rates. The values are shown in Table 2. Model parameters still depend on thermal history, and there is no significant change in shape of the calculated curve in the area where the calculation and experimental results differ. Hence, the presence of a thermal gradient cannot account for the differences in the shape of the recovery curves predicted by the model and those observed experimentally.

In summary, the two problems with the model calculations (i.e., the thermal history dependence of model parameters and the lack of agreement between experiment and model calculations with respect to the shape of annealing peaks) are found to be unaffected by (1) use of a self-consistent equation for the relaxation time and (2) accounting for the effects of thermal gradients. The results suggest that the KWW representation of structural recovery should be reevaluated.

Conclusions

Moynihan's formulation of the Tool−Narayanaswamy structural recovery model was used to describe enthalpy recovery DSC data for poly(ether imide) during heating after cooling at various rates. A self-consistent equation was used to describe the effects of temperature and structure on the relaxation time with one set of parameters capable of describing both glassy and equilibrium behavior. Despite use of this self-consistent equation, model parameters were still dependent on thermal history and there were differences observed between the shape of experimental DSC annealing peaks and model calculations. The presence of a thermal gradient was then incorporated into model calculations. In order to determine the thermal gradient, analytical and numerical calculations of the temperature profile within the DSC sample were performed, taking into account the step change in thermal diffusivity at the glass transition. Thermal gradients were found to significantly affect values of $\tau_{o,ref}$ but not β needed to fit the experimental curves. Thermal gradients cannot account either for the dependence of model parameters on thermal history or for the lack of agreement between the shapes of experimental and calculated DSC annealing peaks.

Acknowledgment. Helpful discussions with Dr. Gregory B. McKenna (NIST) are gratefully acknowledged.

Appendix: Derivation of Temperature Profile

The heat conduction equation[37] governs the change in temperature in the sample

$$\nabla\kappa\,\nabla T = \rho C_p \frac{\partial T}{\partial t} \tag{A1}$$

where κ is the thermal conductivity, ρ is the density, and C_p is the heat capacity of the material. Assuming that the most significant source of heat loss is across the sample thickness (taken as the x-direction), rather than radially, the one-dimensional equation can be solved. Assuming that the thermal conductivity is essentially the same over the entire sample, as discussed in the text, the equation is further simplified

$$\kappa \frac{\partial^2 T}{\partial x^2} = \rho C_p \frac{\partial T}{\partial t} \tag{A2}$$

or

$$k\frac{\partial^2 T}{\partial x^2} = \frac{\partial T}{\partial t} \tag{A3}$$

where k is the thermal diffusivity. The boundary conditions for the symmetrical case at the top and bottom of the sample, at $x = 0$ and L, respectively, are

$$T(x = 0) = T_p(t) = T_o + qt \tag{A4}$$

$$T(x = L) = T_p(t) = T_o + qt \tag{A5}$$

where $T_p(t)$ is the program temperature, T_o is the initial temperature, and q is the rate of change of temperature during the DSC run. The initial condition is assumed to be equal to the initial temperature, although this can be generalized to be any known function of x, as will be shown later:

$$T(x,t=0) = T_o \tag{A6}$$

The solution procedure is similar to that commonly presented in textbooks,[37] with the difference being the difficulties added by the presence of time-dependent boundary conditions. To ease in solution of the differential equation, the boundary conditions were made homogeneous by using the following dimensionless temperature:

$$u = \frac{T - T_p(t)}{T_p(t)} \tag{A7}$$

The other variables are similarly scaled:

$$\xi = \frac{x}{L} \tag{A8}$$

$$\tau = \frac{tk}{L^2} \tag{A9}$$

$$\theta = \frac{L^2 q}{k} \tag{A10}$$

The scaling for time and heating rate implicitly assume that the thermal diffusivity, k, is independent of temperature. Hence, the problem which must be solved is

$$\frac{\partial u}{\partial \tau} + (1+u)\frac{\theta}{T_p(\tau)} = \frac{\partial^2 u}{\partial \xi^2} \tag{A11}$$

$$u(\xi = 0) = 0$$

$$u(\xi = 1) = 0$$

$$u(\tau = 0) = 0$$

The homogeneous problem

$$\frac{\partial u}{\partial \tau} + \frac{u\theta}{T_p(\tau)} = \frac{\partial^2 u}{\partial \xi^2} \tag{A12}$$

was solved by the method of separation of variables. Letting $u(\xi,\tau) = X(\xi)\mathrm{T}(\tau)$, the problem was reduced to solving two differential equations

$$\frac{T'}{T} + \frac{\theta}{T_o + \theta\tau} = \frac{X''}{X} = -\lambda \tag{A13}$$

where $T_o + \theta\tau$ is substituted for $T_p(\tau)$. The variable λ is the separation constant and is not a function of either ξ or τ. Solving these two equations yields

$$T(\tau) = c_1 \frac{e^{-\lambda\tau}}{T_o + \theta\tau} \tag{A14}$$

$$X(\xi) = c_2 \sin(\sqrt{\lambda}\xi) \tag{A15}$$

where the boundary conditions are satisfied with $\sqrt{\lambda} = n\pi$, where $n = 0, 1, 2, 3, \ldots$ Hence, the solution to the homogeneous solution is

$$u = \Sigma\, c_n \frac{e^{-\lambda_n\tau}}{T_o + \theta\tau} \sin(\sqrt{\lambda_n}\xi) = \Sigma T_n(\tau) \sin(\sqrt{\lambda_n}\xi) \tag{A16}$$

To solve the inhomogeneous problem, use was made of the orthogonality of the sine function:

$$T_n(\tau) = 2\int_0^1 u(\xi,\tau) \sin(\sqrt{\lambda_n}\xi)\, d\xi \tag{A17}$$

Taking the derivative with respect to τ, and making substitutions for $\partial u/\partial\tau$, as shown below, a differential equation was obtained for $T_n(\tau)$, which is used to determine the form of c_n

$$\begin{aligned}
\frac{\partial T_n(\tau)}{\partial \tau} &= 2\int_0^1 \frac{\partial u(\xi,\tau)}{\partial \tau} \sin(\sqrt{\lambda_n}\xi)\, d\xi \\
&= 2\int_0^1 \left[\frac{\partial^2 u(\xi,\tau)}{\partial \xi^2} - \frac{u\theta}{T_p(\tau)} - \frac{\theta}{T_p(\tau)}\right] \sin(\sqrt{\lambda_n}\xi)\, d\xi \\
&= 2\int_0^1 \left[-u\lambda_n - \frac{u\theta}{T_p(\tau)} - \frac{\theta}{T_p(\tau)}\right] \sin(\sqrt{\lambda_n}\xi)\, d\xi \\
&= -2\left(\lambda_n + \frac{\theta}{T_p(\tau)}\right) \int_0^1 u \sin(\sqrt{\lambda_n}\xi)\, d\xi - \\
&\qquad \frac{2\theta}{T_p(\tau)} \int_0^1 \sin(\sqrt{\lambda_n}\xi)\, d\xi \\
&= -\left(\lambda_n + \frac{\theta}{T_p(\tau)}\right) T_n(\tau) - \frac{2\theta}{T_p(\tau)} \left[\frac{-\cos n\pi\xi}{n\pi}\right]_0^1 \\
&= -\left(\lambda_n + \frac{\theta}{T_p(\tau)}\right) T_n(\tau) - \frac{4\theta}{T_p(\tau) n\pi}
\end{aligned} \tag{A18}$$

where the last step is true only for $n = 1, 3, 5$, etc. The resulting linear first-order differential equation was solved using an integrating factor to yield:

$$T_n(\tau) = \frac{-4\theta}{n\pi\lambda_n T_p(\tau)} + c_n\, e^{-\lambda_n\tau} \tag{A19}$$

Applying the initial condition, $T_n(\tau) = 0$, gives the form of c_n:

$$T_n(\tau) = \frac{-4\theta}{n\pi\lambda_n T_p(\tau)} (1 - e^{-\lambda_n\tau}) \tag{A20}$$

Thus, the dimensionless temperature, u, in the symmetrical case when the sample temperature is uniform at the beginning of the scan is given by

$$u(\xi,\tau) = \frac{-4\theta}{T_p(\tau)} \sum_{n=1}^{\text{odd}} \frac{(1 - e^{-(n\pi)^2\tau})}{(n\pi)^3} \sin(n\pi\xi) \tag{A21}$$

with the temperature in the sample given by:

$$T(x,t) = T_p(t)(1+u) \tag{A22}$$

References and Notes

(1) Narayanaswamy, O. S. *J. Am. Ceram. Soc.* **1971**, *54*, 491.
(2) Kovacs, A. J. *Ann. N.Y. Acad. Sci.* **1981**, *371*, 38.
(3) Moynihan, C. T.; Macedo, P. B.; Montrose, C. J.; Gupta, P. K.; DeBolt, M. A.; Dill, J. F.; Dom, B. E.; Drake, P. W.; Esteal, A. J.; Elterman, P. B.; Moeller, R. P.; Sasabe, H.; Wilder, J. A. *Ann. N.Y. Acad. Sci.* **1976**, *15*, 279.
(4) Hodge, I. M. *J. Non-Cryst. Solids* **1994**, *169*, 211.
(5) O'Reilly, J. M. *CRC Crit. Rev. Solid State Mater. Sci.* **1987**, *13* (3), 259.
(6) Rendell, R. W.; Aklonis, J. J.; Ngai, K. L.; Fong, G. R. *Macromolecules* **1987**, *20*, 1070.
(7) McKenna, G. B. In *Comprehensive Polymer Science*; Booth, C., Price, C., Ed.; Pergamon: Oxford, England, 1989; Volume 12, Polymer Properties.
(8) Foltz, C. R.; McKinney, P. V. *J. Appl. Polym. Sci.* **1969**, *13*, 2235.

(9) Petrie, S. E. B.; *J. Polym. Sci., Part A-2* **1972**, *10*, 1255.
(10) Struik, L. C. E. *Physical Aging in Amorphous Polymers and Other Materials*; Elsevier: Amsterdam, 1978.
(11) Moynihan, C. T.; Crichton, S. N.; Opalka, S. M. *J. Non-Cryst. Solids* **1991**, *131−133*, 420.
(12) McKenna, G. B.; Angell, C. A.; *J. Non-Cryst. Sol.* **1991**, *133−133*, 528.
(13) Hodge, I. M.; Huvard, G. S. *Macromolecules* **1983**, *16*, 371.
(14) Hutchinson, J. M.; Ruddy, M.; Wilson, M. R. *Polymer* **1988**, *29*, 152.
(15) Kolrausch, F. *Pogg. Ann. Phys.* **1847**, *12*, 393.
(16) Williams, G.; Watts, D. C. *Trans. Faraday Soc.* **1970**, *66*, 80.
(17) Moynihan, C. T.; Esteal, A. J.; Wilder, J.; Tucker, J.; *J. Phys. Chem.* **1974**, *78*, 2673.
(18) O'Reilly, J. M.; Hodge, I. M. *J. Non-Cryst. Solids* **1991**, *131−133*, 451.
(19) Richardson, M. J.; Burrington, P. *J. Therm. Anal.* **1974**, *6*, 345.
(20) Lagasse, R. R. *J. Polym. Sci.: Polym. Phys.* **1982**, *20*, 279.
(21) Mraw, S. C. *Rev. Sci. Instrum.* **1982**, *53*, 228.
(22) Debolt, M. A. Ph.D. Thesis, Catholic University of America, Washington, DC, 1976.
(23) Donoghue, E.; Ellis, T. S.; Karasz, F. E. In *Analytical Calorimetry*; Gioll, P., Ed., Plenum: New York, 1984; Vol 5.
(24) Tool, A. Q. *J. Am. Ceram. Soc.* **1946**, *29*, 240.
(25) Moynihan, C. T.; et al. *J. Am. Ceram. Soc.* **1976**, *59*, 12.
(26) Vogel, H. *Phys. Z.* **1921**, *22*, 645.
(27) Williams, M. L.; Landell, R. F.; Ferry, J. D. *J. Am . Chem. Soc.* **1955**, *77*, 3701.
(28) Sherer, G. W. *J. Am. Ceram. Soc.* **1984**, *67*, 504.
(29) Adam, G.; Gibbs, J. H. *J. Chem. Phys.* **1965**, *43*, 139.
(30) DiMarzio, E. A.; Dowell, F. *J. Appl. Phys.* **1979**, *50*, 6061.
(31) Goldstein, M. J. *J. Chem. Phys.* **1976**, *64*, 4767.
(32) Roe, R.-J.; Tonelli, A. E. *Macromolecules* **1978**, *11*, 114.
(33) Echeverria, I.; Su, P.-C.; Simon, S. L.; Plazek, D. J. *J. Polym. Sci.: Part B: Polym. Phys.* **1995**, *33*, 2457.
(34) Hodge, I. M. *Macromolecules* **1987**, *20*, 2897.
(35) Matsuoka, S. *Relaxation Phenomena in Polymers*; Oxford University Press: New York, 1992.
(36) Spathis, G. *Polymer* **1994**, *35*, 791.
(37) *Elementary Differential Equations and Boundary Value Problems*; Boyce, W. E.; DiPrima, R. C., John Wiley and Sons: New York, 1986.
(38) Orwoll, R. A. In *Physical Properties of Polymers Handbook*; Mark, J. E. Ed.; American Institute of Physics: Woodbury, NY, 1996; Chapter 7.
(39) Wen, J. In *Physical Properties of Polymers Handbook*; Mark, J. E., Ed.; American Institute of Physics, Woodbury, NY, 1996; Chapter 9.
(40) Pattnaik, S.; Thompson, E. V. *Polym. Prepr. 22*.
(41) Yang, Y. In *Physical Properties of Polymers Handbook*; Mark, J. E., Ed., American Institute of Physics: Woodbury, NY, 1996; Chapter 10.
(42) Simon, S. L.; Plazek, D. J.; Sobieski, J. W.; McGregor, E. T. *J. Polym. Sci. Part B: Polym. Phys.* **1997**, *35*, 929.
(43) Menczel, J. D.; Leslie, T. M. *Thermochim. Acta* **1990**, *166*, 309.
(44) Biddlestone, F.; Goodwin, A. A.; Hay, J. N.; Mouledous, G. A. C. *Polymer* **1991**, *32*, 3119.
(45) Hutchinson, J. M.; Ruddy, M. *J. Polym. Sci., Part B: Polym. Phys.* **1990**, 28, 2127.
(46) In an MRS preprint, the value of β was reported by the same author to decrease slightly rather than to increase on incorpoartion of thermal gradients. This was because ΔC_p-(T) in eq 3 was taken at the program temperature rather than at the average sample temperature.

MA9614508